JOURNAL OF GEOPHYSICAL RESEARCH, VOL. 104, NO. E5, PAGES 11,817–11,826, MAY 25, 1999

Io's patchy SO_2 atmosphere as measured by the Galileo ultraviolet spectrometer

A. R. Hendrix, C. A. Barth, and C. W. Hord

Laboratory for Atmospheric and Space Physics, University of Colorado, Boulder

Abstract. The Galileo ultraviolet spectrometer has observed Jupiter's volcanically active moon Io in the 2100-3200 Å wavelength range at 13.7 Å resolution. We find that both sulfur dioxide frost on the surface and sulfur dioxide gas in Io's atmosphere are detectable. Io's SO_2 atmosphere is not hemispherically homogeneous, but is patchy, with both thick and thin regions. During an observation near 120-150°W longitude, we find that a thick SO_2 atmosphere (column density $N=1.0x10^{19}$ cm^{-2}) covers ~35% of the observed region, while a thinner SO_2 ($N=4.0x10^{17}$ cm^{-2}) atmosphere covers 25% of the observed region. The thick atmospheric component is significant in the 2350-2400 Å range, while the thinner component is important particularly at wavelengths shorter than ~2300 Å. Likely sources of the SO_2 atmosphere are volcanic plumes and sublimation of SO_2 frost, as well as outgassing associated with the several hotspots in the field of view.

1. Introduction

The primary sources of Io's atmosphere are sublimation of surface SO_2 frost and volcanic plumes. In the first close-up observations of Io since Voyager, we show that Io's atmosphere consists of both thick and thin components. In this analysis of Io data, using spectra from the Galileo ultraviolet spectrometer (UVS), we look at a larger wavelength range (2100 - 3200 Å) than in earlier International Ultraviolet Explorer (IUE) and Hubble Space Telescope (HST) observations; furthermore, we do not focus on the fine structure of the SO_2 gas, but on the broad shape of the SO_2 cross section. We use the knowledge that SO_2 frost reflectance and SO_2 gas cross section have unique shapes in this wavelength range. We allow for both thick and thin SO_2 gas components and derive the best fit column densities of both. We find that Io's ultraviolet albedo is explained not only by SO_2 frost, but also by an SO_2 gas component overlying the frost with a column density $N=4.0x10^{17}$ cm^{-2}. Surrounding the frost region are several hotspots; associated with these hotspots is a thicker SO_2 gas component with a column density of $N=1.0x10^{19}$ cm^{-2}.

2. Background

Io's SO_2 atmosphere has been measured by many instruments in several wavelength regions; differing results have been obtained. Here we summarize these past results; later we will compare the UVS results to those presented here.

The arrival of Voyager at Io in 1979 brought the discovery of the existence of active volcanoes and the presence of gaseous SO_2. Ground-based observations had already confirmed the presence of SO_2 frost on the surface [*Cruikshank et al.*, 1978; *Pollack et al.*, 1978; *Fanale et al.*, 1979; *Smythe et al.*, 1979]. The infrared interferometer spectrometer (IRIS) on Voyager measured gaseous SO_2 at 1000-1500 cm^{-1} and determined that the column density (N) of Io's SO_2 equilibrium (ambient) atmosphere was $5.4x10^{18}$ cm^{-2} [*Pearl et al.*, 1979]. (*Lellouch et al.* [1992] showed that the inferred column density could also be ~$3x10^{17}$-$2x10^{18}$ cm^{-2} due to non-local thermodynamic equilibrium (LTE) effects.) The IUE was used by *Bertaux and Belton* [1979] in the 2400-3400 Å range to determine an upper limit on Io's disk-averaged SO_2 atmospheric column density of $4.2x10^{17}$ cm^{-2}, and by *Butterworth et al.* [1980] in the 2900-3100 Å wavelength range to determine an upper limit for the thickness of Io's atmosphere at $2.1x10^{17}$ cm^{-2}. However, it was determined by *Belton* [1982] that the *Butterworth et al.* [1980] measurements did not have the resolution necessary to adequately identify gaseous SO_2 in the 2900-3100 Å wavelength range, where Beer's law may be inadequate to describe the transmission of SO_2 gas. *Howell et al.* [1989] determined an upper limit on the SO_2 abundance at $2.7x10^{18}$ cm^{-2} using ground-based spectra near 4 μm.

More recently, *Ballester et al.* [1990] used IUE to make high spectral resolution observations of Io near 3000 Å. They found that, for both Io's leading and trailing hemispheres, the upper limit on the average SO_2 column density was $2.0x10^{17}$ cm^{-2} for a homogeneous atmosphere. *Lellouch et al.* [1992] observed both the leading and trailing hemispheres of Io using millimeter wavelengths. They found a typical column density of $6.0x10^{17}$ cm^{-2} covering 5-20% of Io's surface. *Ballester et al.* [1994] used the HST Faint Object Spectrograph (FOS) to make high spectral resolution observations of Io's trailing hemisphere in the 2000-2300 Å range. They found that hemispheric atmospheres have an average column density of 6-$10x10^{15}$ cm^{-2}, while better fits were obtained with more confined atmospheres (~8% of disk centered on the subsolar point) of ~$3x10^{17}$ cm^{-2}. *Trafton et al.* [1996] observed Io with the HST Goddard High Resolution Spectrograph (GHRS) to obtain very high resolution spectra in the 2095-2135 Å range. They found that, for a homogeneous atmosphere, the trailing hemisphere had a column density of $N=6.7x10^{15}$ cm^{-2} while the column density for the leading hemisphere was found

Paper number 1999JE900009.
0148-0227/99/1999JE900009$09.00

to be N=4.9x10^{15} cm^{-2}. More confined atmospheric regions (covering ~35% of the disk in the center of the disk) had column densities of 2.1x10^{17} cm^{-2}. Denser localized atmospheres were measured using the HST Faint Object Camera (FOC) at 2850 Å [*Sartoretti et al.*, 1994] and at 2325 Å, 2600 Å and 2850 Å [*Sartoretti et al.*, 1996]. They measured column densities of ~1x10^{18} cm^{-2} in patches covering 11-15% of the observed regions, along with SO_2 frost on the surface of Io. The results of these observations are summarized in Table 1.

Lellouch [1996], in an excellent review paper, compared the UV (near 2100 Å) and millimeter wavelength results and suggested that the UV wavelengths detect a thin localized component (N~5x10^{15}-5x10^{16} cm^{-2}), associated with sublimation of SO_2 frost, while millimeter wavelength data detect a thicker localized component (N~5x10^{16}-5x10^{17} cm^{-2}), due to volcanic plumes. However, it was acknowledged that the modeling of the millimeter wavelength data was still uncertain, and *Lellouch* [1996] concluded that the nature of Io's atmosphere is still somewhat unclear.

3. Observations

The Galileo UVS was built at the University of Colorado's Laboratory for Atmospheric and Space Physics and is described by *Hord et al.* [1992]. It consists of a Cassegrain telescope used to collect light and an Ebert-Fastie scanning

Table 1. Summary of Previous Io Atmosphere Results

Reference	Instrument	Wavelength Range	Longitude	Derived Column Density, cm^{-2}	Notes
Pearl et al. [1979]	Voyager IRIS	7 μm	~300°W	5.4x10^{18}	over Loki plume
Bertaux and Belton [1979]	IUE	2400-3400 Å		<4.2x10^{17}	disk-average
Butterworth et al. [1980]	IUE	2900-3100 Å	80-90°W	<2.4x10^{17}	disk-average
Howell et al. [1989]	ground-based	4 μm	70°W	<2.7x10^{18}	
Ballester et al. [1990]	IUE	2900-3150 Å	114°W, 305°W	2.0x10^{17}	hemispheric
Lellouch et al. [1992]	ground-based	mm-wave	LH	~1.6x10^{17}	covering ~5-20% of disk
			TH	~1.2x10^{18}	covering ~5-20% of disk
Clarke et al. [1994]	HST GHRS	2300-3300 Å	330°W	<4x10^{16}	disk-average
				2x10^{19}	over 10%
				2x10^{16}	over 90%
Ballester et al. [1994]	HST FOS	2000-2300 Å	278°W, 292°W	6-10x10^{15}	hemispheric
				3x10^{17}	center of disk
Sartoretti et al. [1994]	HST FOC	2850 Å, ~4500 Å	TH (270°-284°W)	~1x10^{18}	covering 13% of disk
			LH (67°W)	~1x10^{18}	covering 0% of disk
Trafton et al. (1996)	HST GHRS	2095-2135 Å	80°-97°W	4.9x10^{15}	LH hemispheric
			171°-285°W	6.7x10^{15}	TH hemispheric
				2.1x10^{17}	covering 35% of disk, LH and TH
Sartoretti et al. [1996]	HST FOC	2325, 2600, 2850 Å	LH (68°W-133°W)	~1x10^{18}	covering ~11-15% of disk
			TH (233°W-270°W)	~1x10^{18}	covering ~11-15% of disk

LH, leading hemisphere, centered on 90°W longitude; TH, trailing hemisphere, centered on 270°W longitude

spectrometer. A diffraction grating scans the ultraviolet spectrum, and three photomultiplier tubes record the signal. The data reported here were acquired using the F channel, which covers the 1620 - 3231 Å wavelength region with a spectral resolution of 13.7 Å; the sampling is performed every 3.1 Å. The calibration of the F channel is described by *Hendrix* [1996]. The entire spectrum is scanned in 4.33 s, with a 0.006 s integration period for each of the 528 grating positions. The instantaneous angular size of the slit is 0.1° x 0.4°.

The observation described in this paper was performed on May 31, 1998. During this observation, the UVS F channel field of view (FOV) was held steady on Io's surface centered near 130°W longitude. The central portion of the FOV covered part of Bosphorus Regio, which, as shown by *Lopes-Gautier et al.* [1997], is a bright region (likely SO_2 frost) surrounded by hot spots. The phase angle during the observation (averaged over the FOV) was 51°, and the subsolar point was near 90°W. The emission and incidence angles, averaged over the FOV, were 43.8° and 40.5°, respectively. As shown in Plate 1, the length of the FOV was approximately one Io diameter. The observation lasted 56 min, during which 784 spectra were summed. Figure 1a displays the measured reflectance. In Figure 1a (and other figures) the UVS-measured spectrum is shown in 15 Å bins.

4. Photometric Corrections

To convert from a measured reflectance to an albedo, we corrected for observational geometry using the Hapke photometric function [*Hapke*, 1993]:

$$r_m(\mu, \mu_0, \alpha, \lambda) = \omega(\lambda)\frac{\mu_0}{\mu + \mu_0}[(1+B(\alpha,\lambda))p(\alpha)]R(\bar{\Theta},\alpha) \quad (1)$$

Although we are investigating the amount of SO_2 gas in Io's atmosphere, and Hapke's model applies to surfaces, we use this function because we detect both the surface and the atmospheric components. In (1), $r_m(\mu, \mu_0, \alpha, \lambda)$ is the measured reflectance, $\omega(\lambda)$ is the single-scatter albedo, μ and μ_0 are the cosines of the emission and incidence angles, respectively, $B(\alpha, \lambda)$ accounts for the opposition surge, $R(\bar{\Theta}, \alpha)$ corrects for surface roughness, and $p(\alpha)$ is the phase correction. (All terms are discussed by *Hapke* [1993].) We used (1) to solve for the single-scatter albedo as it varies with wavelength.

The measured reflectance $r_m(\mu, \mu_0, \alpha, \lambda)$ is determined by calibrating the measured spectra by dividing by the calibration curve for the F channel [*Hendrix*, 1996] and removing reflected solar features by dividing by the solar spectrum. We used a solar spectrum measured by the UARS Solar Stellar Irradiance Comparison Experiment (SOLSTICE) instrument [*Rottman et al.*, 1993]. The solar flux in the 2000-3200 Å region varies by less than 1.5% over the solar cycle, so our results are not significantly affected by using a solar spectrum measured on a different day than the UVS Io observation. The solar spectrum, originally at 0.1 nm resolution, was double-boxcar smoothed to match the resolution of the UVS and interpolated to the UVS wavelength scale.

Io's ultraviolet photometric parameters have not been previously determined, although visible photometric parameters have been derived by *Simonelli and Veverka* [1984, 1986] and *McEwen et al.* [1988]. The surface roughness parameter $\bar{\Theta}$ is not expected to vary with wavelength, so we used the value determined by *McEwen et al.* [1988], $\bar{\Theta}$=30°. We also tried varying the value of the opposition effect term B_0, but since our smallest phase angle is 13°, we found we could not constrain that parameter and used B_0=0.

To determine the best phase curve parameters to apply to the UVS Io spectrum, we used the double-lobed Henyey-Greenstein phase function of (2) in the Hapke model and compared the resultant Hapke model to the UVS-measured Io reflectances at various phase angles to find the best fit values of b and c.

$$p(\alpha) = \frac{(1-c)(1-b^2)}{(1-2b\cos\alpha + b^2)^{3/2}} + \frac{c(1-b^2)}{(1+2b\cos\alpha + b^2)^{3/2}} \quad (2)$$

To derive the ultraviolet phase curve, we used 14 UVS Io observations, previously described by *Hendrix et al.* [1996, 1997], which covered the 13° -113° phase angle range. The observations were taken at several different longitudes on Io's leading hemisphere (longitudes 0-180°W). By comparing the Hapke model (with different combinations of b and c values) with the measured reflectances, we found the best fit values of b and c to be -0.50 and 0.85, respectively. The values of b and c did not vary appreciably with wavelength and did not affect the derived albedos outside of the statistical error bars. We also attempted to use the single-lobed Henyey-Greenstein phase function but found that it inadequately fit the high-phase angle observation (α=113°); Io is more forward scattering at high phase angles than the single-lobed phase function predicted, likely due to volcanic particles.

In Figure 1b we show the Hapke model plotted along with UVS-measured reflectances of Io's leading hemisphere at various phase angles. The data in Figure 1b are for 2900 Å, and we find that the photometric parameters making up this Hapke model (with the exception of the single-scatter albedo) are reasonable for all wavelengths in the 2100-3200 Å region.

To compare the data with atmospheric models, we converted from the derived single-scatter albedo ω to the geometric albedo using (3) from *Hapke* [1993, p. 353]:

$$ga(\lambda) = \frac{\omega}{8}\{[1+B_0]p(0)-1\}+U(\bar{\Theta})\frac{r_0}{2}(1+\frac{r_0}{3}) \quad (3)$$

In (3), $ga(\lambda)$ is the geometric albedo, U is an empirical term accounting for macroscopic roughness (given by *Hapke* [1993, p. 353]) and r_0 is the diffusive reflectance [*Hapke*, 1993, p. 196]. Using the photometric corrections of (1)-(3), we obtain a geometric albedo comparable to the HST measurement of *Clarke et al.* [1994]. The derived geometric albedo is shown in Figure 1c. The geometric albedo is provided in tabular form in Table 2.

5. Models

In this study, we fit three different models to the derived Io albedo. The three models are outlined in Table 3 and described below. The results of the models are shown in Table 4. We quantitatively analyze the fit of the model to the data by minimizing χ^2 over the 2100-3200 Å wavelength range:

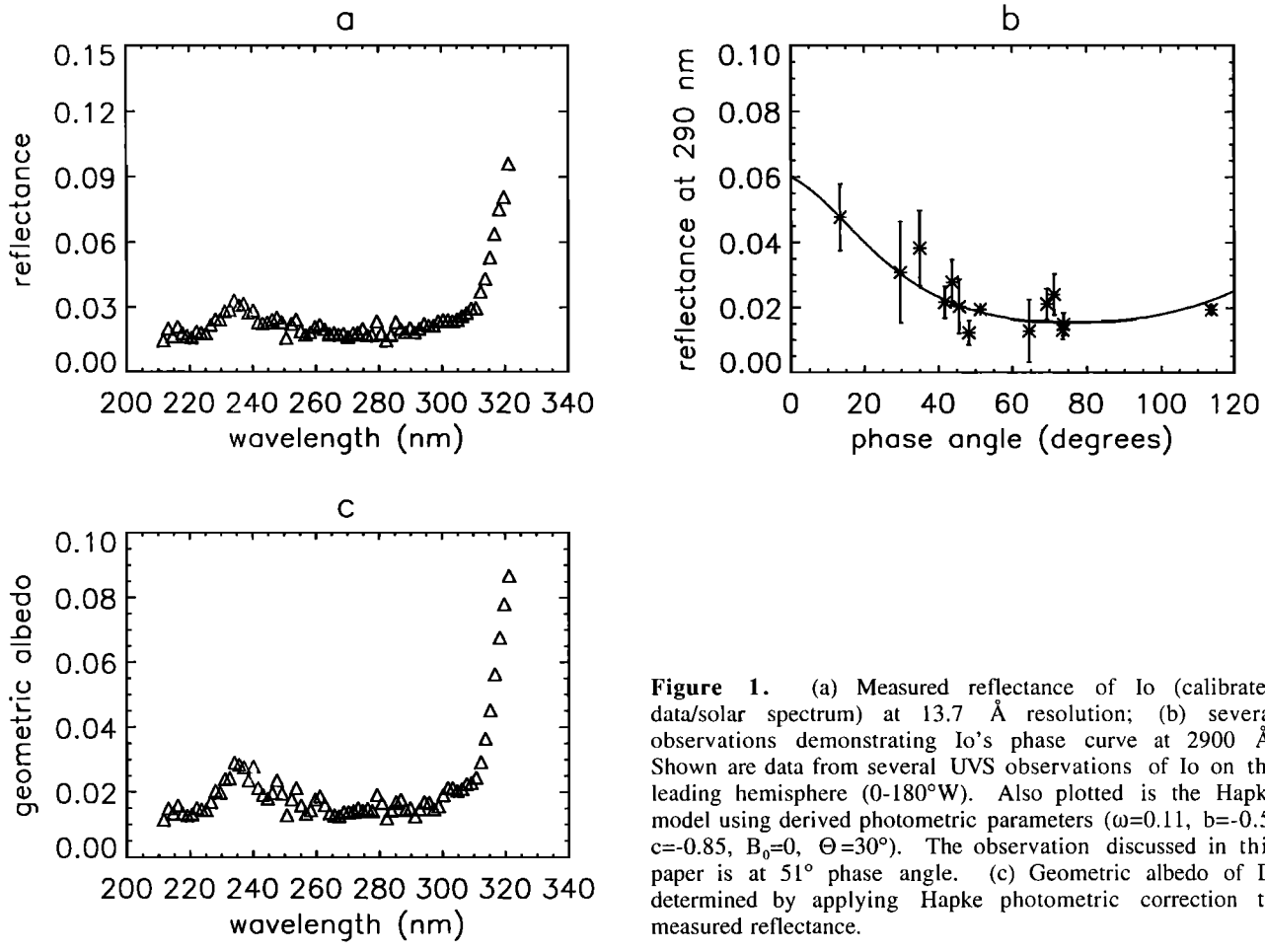

Figure 1. (a) Measured reflectance of Io (calibrated data/solar spectrum) at 13.7 Å resolution; (b) several observations demonstrating Io's phase curve at 2900 Å. Shown are data from several UVS observations of Io on the leading hemisphere (0-180°W). Also plotted is the Hapke model using derived photometric parameters (ω=0.11, b=-0.5, c=-0.85, B_0=0, Θ=30°). The observation discussed in this paper is at 51° phase angle. (c) Geometric albedo of Io determined by applying Hapke photometric correction to measured reflectance.

$$\chi^2 = \Sigma \frac{\text{abs(model} - \text{ga)}}{\text{ga}} \quad (4)$$

5.1 Model Components

Figure 2 displays the important components of our models, SO_2 frost reflectance and SO_2 gas cross section. The frost and gas are spectrally distinct in this wavelength range. As shown in Figure 2a, SO_2 frost increases sharply in reflectance between 3000 and 3200 Å. Between 3000 and 2000 Å, the reflectance increases slightly with decreasing wavelength. There is a broad local maximum in reflectance near 2350-2400 Å. For SO_2 gas, Figure 2c shows that column densities near 5×10^{16} cm^{-2} are best detected shortward of 2300 Å and are practically undetectable at longer wavelengths. As the column density increases, the transmission of the gas decreases overall, and the maximum in transmission near 2350-2400 Å becomes more narrow. Also, as column density increases, the fine band structure near 2100 Å increases and the bands become stronger. At column densities near 5×10^{18} cm^{-2}, these bands saturate out and the reflectance in that wavelength region is black.

Comparing the spectra in Figures 2a and 2c to the albedo in Figure 1c, we see that Io displays a sharp increase in albedo between 3000 and 3200 Å, consistent with SO_2 frost. At other wavelengths, Io's albedo is generally flat, except for a maximum near 2350-2400 Å. This feature appears to be too narrow to be accounted for by the SO_2 frost, which has a much broader local maximum in reflectance (Figure 2a). In contrast, the feature is consistent with the narrow local maximum in transmission of a thick SO_2 column (Figure 2c).

In the models described here, we used a medium-grain (~100-200 μm) SO_2 frost reflectance (Figure 2a). The SO_2 frost reflectance was from *Wagner et al.* [1987], scaled to agree with the medium-grain SO_2 frost data from *Nash et al* [1980]. *Carlson et al.* [1997] found that the size of the SO_2 frost grains in Io's equatorial regions is of the order 300 μm, and because most of the reflectance from Io's surface during the UVS observations was from the equatorial regions, this comparison should be adequate. The SO_2 gas cross section used in this study (at 293±10K) was from *Manatt and Lane* [1993]; it is shown in Figure 2b degraded to the UVS spectral resolution. It is unclear how much the use of room-temperature SO_2 cross sections in our Io atmosphere model affects our results. The temperature of Io's atmosphere is uncertain; *Ballester et al.* [1994] obtained temperatures between 110 and 250 K for constrained SO_2 atmospheres, while *Lellouch et al.* [1992] found temperatures as high as 500-600 K.

5.2 Model 1: Surface Reflectance Only

Model 1 accounts only for surface reflectance and ignores any gaseous sulfur dioxide. In Model 1, we fixed the amount of SO_2 frost on the surface (X_1 in Table 3) at 35%. This amount was based on comparing the amount of the FOV filled with the

Table 2. Geometric Albedo

Wavelength, Å	Albedo	Wavelength, Å	Albedo	Wavelength, Å	Albedo
2115.83	0.0119	2491.58	0.0203	2867 33	0 0184
2130.86	0.0156	2506.61	0.0134	2882.36	0.0151
2145.89	0.0140	2521.64	0.0185	2897.39	0.0156
2160.92	0.0165	2536.67	0 0221	2912.42	0.0131
2175.95	0.0139	2551.70	0.0165	2927.45	0.0154
2190.98	0.0133	2566.73	0.0139	2942.48	0.0177
2206.01	0.0138	2581.76	0.0150	2957.51	0.0174
2221.04	0.0157	2596.79	0.0184	2972.54	0.0153
2236.07	0.0151	2611.82	0.0194	2987.57	0.0163
2251.10	0.0151	2626.85	0.0167	3002.60	0.0199
2266.13	0.0176	2641.88	0.0140	3017.63	0.0222
2281.16	0.0212	2656.91	0.0134	3032.66	0.0221
2296.19	0.0206	2671.94	0.0132	3047.69	0.0212
2311.22	0.0250	2686.97	0.0144	3062.72	0.0219
2326.25	0.0253	2702.00	0.0144	3077.75	0.0235
2341.28	0.0303	2717.03	0.0147	3092.78	0.0238
2356.31	0.0297	2732.06	0.0156	3107.81	0.0256
2371.34	0.0289	2747.09	0.0148	3122.84	0.0305
2386.37	0.0246	2762.12	0.0155	3137.87	0.0381
2401.40	0.0290	2777.15	0.0148	3152.90	0.0472
2416.43	0.0222	2792.18	0.0200	3167.93	0.0587
2431.46	0.0199	2807.21	0 0173	3182.96	0.0706
2446.49	0.0187	2822.24	0.0125	3197.99	0.0814
2461.52	0.0205	2837.27	0.0149	3213.02	0.0906
2476.55	0.0246	2852.30	0.0176		

Table 3. Models

Model	Description
1. Surface reflectance only	albedo=$X_1R_{SO2} + X_2R_{other}$ X_1= percent coverage by SO_2 frost R_{SO2}= reflectance of SO_2 frost X_2= percent coverage by other component (X_2= 100% - X_1) R_{other}= reflectance of other component
2: Hemispheric atmosphere	albedo=$(X_1R_{SO2} + X_2R_{other})S$ S= transmission of SO_2 gas (see text)
3: Patchy atmosphere	albedo=$X_1R_{SO2}S_1 + X_2R_{other}S_2 + X_3R_{other}$ S_1= transmission by atmospheric component overlying SO_2 frost S_2= transmission by atmospheric component overlying other surface material X_3= 100%-X_1-X_2= region of surface coverage by other surface material and no gas= 40%

Table 4. Results

	% SO_2 Frost (Set)	R_{other}	Hemispheric Column Density N, cm^{-2}	Percent Thick SO_2 Gas Coverage	Thick SO_2 Column Density N, cm^{-2}	Percent Thin SO_2 Gas Coverage	Thin SO_2 Column Density N, cm^{-2}	χ^2
model 1	35%	0.018						13.1
model 2	35%	0.020	5.0e16					10.6
model 3	35%	0.032		25%	1.0e19	35%*	4 0e17	9.1

* overlying SO_2 frost

bright material in solid state imaging (SSI) camera images, which covers approximately ±15° latitude. This is also in agreement with the results of *McEwen et al.* [1988] for this longitude region. We then solved for the best fit reflectance of another surface material, covering the regions void of SO_2 frost, which we assumed had no variation in reflectance with wavelength (R_{other} in Table 3).

The result of this model is shown in Figure 3a. The best fit value of R_{other} was 0.018. Figure 3a shows that this model accounts for the steep increase in albedo near 3100 Å (attributable to SO_2 frost) but does not simulate the other features in the measured albedo, which we find from Model 3 are due to SO_2 gas of varying thicknesses. The importance of this model is to demonstrate that SO_2 gas is indeed detectable in this wavelength range.

5.3 Caveats

Models 2 and 3 include transmission by SO_2 gas, which requires an introduction before we explain those models and

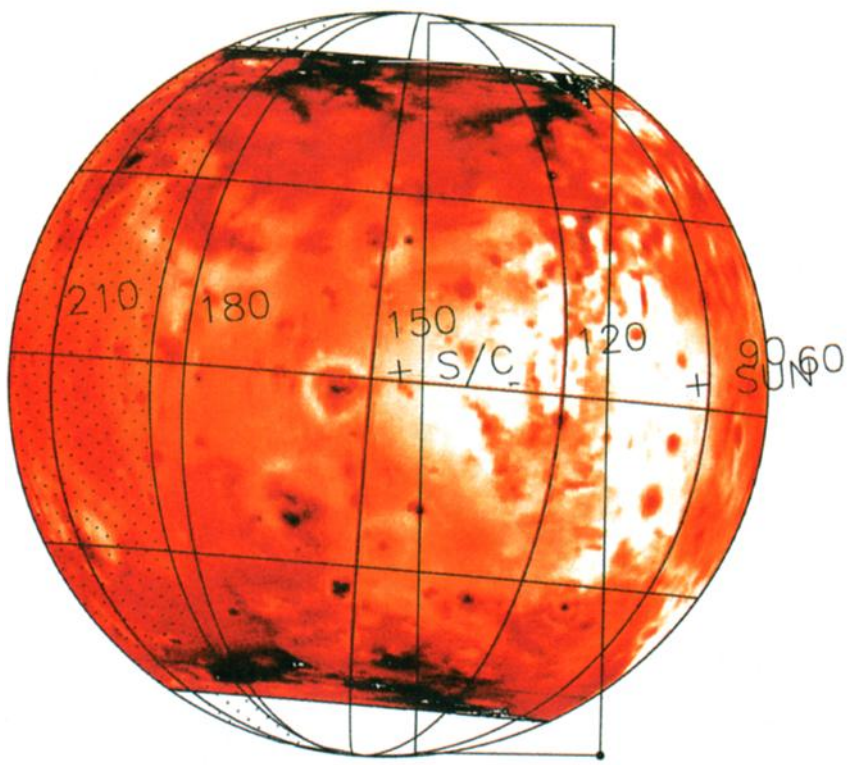

Plate 1. Image of the UVS Io observation indicating the region observed. The FOV was held in this position for 56 min; the 784 spectra acquired during the observation were averaged and used in the analysis to determine the albedo of the region observed. The observed region includes SO_2 frost-rich Bosphorus Regio (~15°S-15°N) and several hotspots in the 15°S-30°S and 15°N-30°N regions.

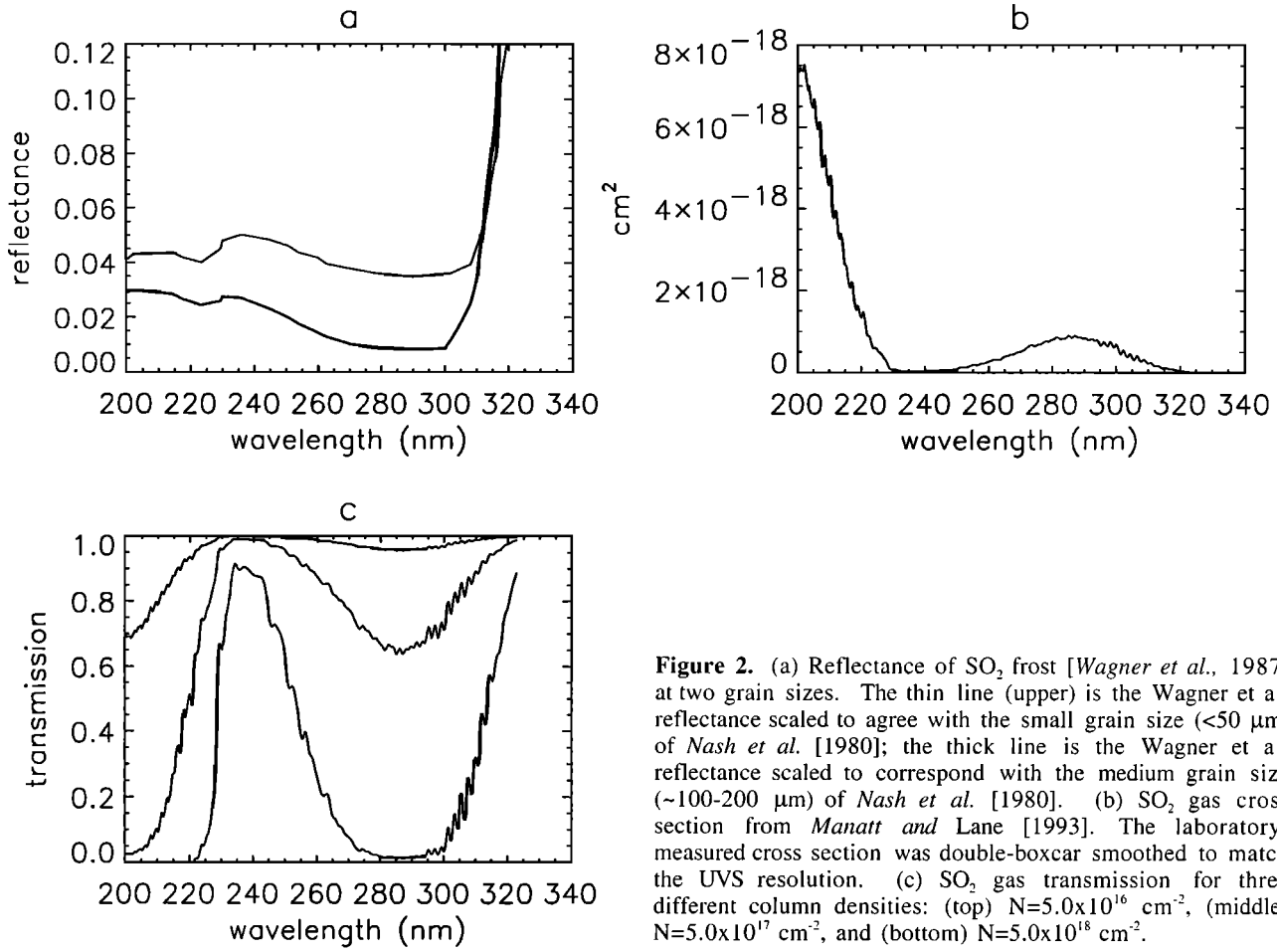

Figure 2. (a) Reflectance of SO_2 frost [*Wagner et al.*, 1987] at two grain sizes. The thin line (upper) is the Wagner et al. reflectance scaled to agree with the small grain size (<50 μm) of *Nash et al.* [1980]; the thick line is the Wagner et al. reflectance scaled to correspond with the medium grain size (~100-200 μm) of *Nash et al.* [1980]. (b) SO_2 gas cross section from *Manatt and* Lane [1993]. The laboratory-measured cross section was double-boxcar smoothed to match the UVS resolution. (c) SO_2 gas transmission for three different column densities: (top) N=5.0x10^{16} cm^{-2}, (middle) N=5.0x10^{17} cm^{-2}, and (bottom) N=5.0x10^{18} cm^{-2}.

results. *Belton* [1982] pointed out that, due to the densely packed nature of the spectral lines in the SO_2 cross section, Beer's law may not be an appropriate approximation for the transmission of this gas.

Ballester et al. [1994] provide an in-depth investigation of methods to use to account for curve-of-growth effects due to the crowded SO_2 lines in the 2100 Å region. Instead of using Beer's law, they applied a Malkmus model with a given k distribution to determine column densities of SO_2 measured at Io in high-resolution HST spectra. This method solves the

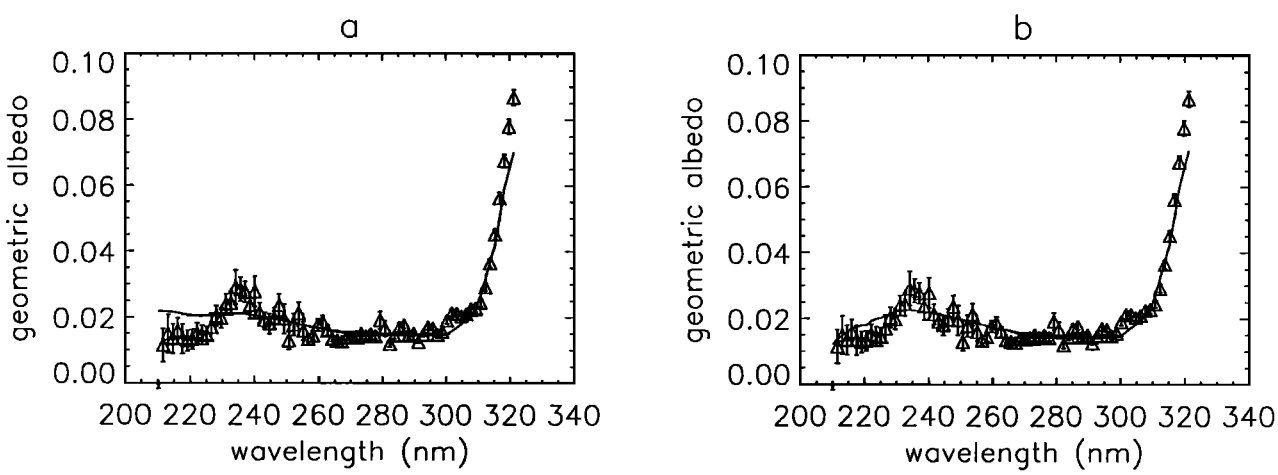

Figure 3. Ultraviolet albedo of Io as measured by the UVS. Measured albedo is shown as triangles in 15 Å bins, while model is shown as a solid line. Error bars are due to statistical error in the measurement. Comparison with (a) Model 1 (surface reflectance only), where the best fit model included 35% SO_2 frost and 65% of a flat 0.018 reflectance; and (b) Model 2 (surface reflectance plus hemispheric SO_2 atmosphere), where the best fit model included 35% SO_2 frost plus 65% flat reflectance of 0.020 and a hemispheric SO_2 atmosphere of column density N=5.0x10^{16} cm^{-2}.

problem of not knowing the cross section exactly in regions where the line spacing is small. *Clarke et al.* [1994], in analyzing a HST GHRS spectrum of Io in the 2300-3300 Å region effectively ignored the problem by stating that the cross section had not been measured well enough at near-UV wavelengths, and they used Beer's law in their approximations of the thickness of Io's atmosphere.

We used a combination of these two methods. For wavelengths between 2100 and 2300 Å we used the Malkmus model described by *Ballester et al.* [1994]:

$$S = \exp\left(-\frac{\pi}{2} y\left[\left(1+\frac{4\bar{\sigma}}{\pi y}N\right)^{1/2}-1\right]\right) \quad (5)$$

where we use y=1.85 over this wavelength range, as obtained by *Ballester et al.* [1994] near 2100 Å for a particular k distribution. In the 2300-3250 Å range, we used Beer's law to determine the best fit column densities. We also tried using the Malkmus model in this wavelength range; however, the y value is unknown here due to a lack of high-resolution laboratory measurements of the SO_2 cross section in this range. When we simply used y=1.85 over the entire wavelength range, we obtained the same best fit column densites as when we used Beer's law. As will be shown, the range of values of column densities derived in this analysis is larger than the possible error due to using Beer's law versus a random band model.

5.4 Model 2: Homogeneous SO_2 Gas

In Model 2 we allowed for surface reflectance by SO_2 frost and another component (as in Model 1), as well as transmittance by SO_2 gas distributed homogeneously across the observed region. In Model 2, we fixed the percent coverage by SO_2 frost at 35% and solved for the best fit values of the reflectance of the other surface component and the best fit column density (N) of the SO_2 gas. We accounted for the average slant angle to the observed region by incorporating the average μ and μ_0 (cosine of emission and incidence angles, respectively) values over the FOV into the transmission part of Model 2, where the two-way absorption $Z=(1/\mu+1/\mu_0)N$.

The best fit model ($N=5.0\times10^{16}$ cm^{-2}) shown in Figure 3b shows that a homogeneous atmosphere improves the fit to the data over Model 1 but still does not account for the maximum in albedo near 2350 Å. Adding gaseous SO_2 also means that a brighter surface reflectance (other than SO_2 frost) is required: a flat 0.020 reflectance fits the data best. It is not expected that SO_2 gas would be distributed homogeneously across the observed region with its varying sources of gas such as SO_2 frost, hotspots, and nearby volcanic plumes. However, we include the results of this model here to demonstrate the effects of including patchy regions of thick and thin atmospheric components (Model 3).

5.5 Model 3: Patchy Atmosphere

Model 3 allows for surface reflectance by SO_2 frost and another component (as in Model 1), as well as transmittance by both a localized relatively dense SO_2 atmosphere and a thin SO_2 atmosphere component. We fixed the percent coverage by SO_2 frost at 35% covering the central part of the FOV. We allowed the rest of the FOV to be covered by a surface component of reflectance R_{other}. We allowed two atmospheric components to exist: a "thick" component ($N>1\times10^{18}$ cm^{-2}) and a "thin" component ($N<1\times10^{18}$ cm^{-2}). We tried different amounts of coverage by the thick and thin components while keeping X_I=35%, corresponding to Bosphorous Regio between ~15°S and 15°N. We did not allow the gaseous SO_2 to extend beyond 30° latitude; higher latitude regions were assumed covered by the nonfrost surface material and had no gas coverage. In this way, gas was allowed to cover 60% of the observed region. For instance, we tried allowing the thick gas component to cover the entire 35% of the frost portion of the FOV, while the thin gas component covered 25% of the FOV over the nonfrost material, and the remaining 40% had no gas coverage. We tried many combinations of thick and thin gas component coverage, while keeping the frost coverage constant at 35% and the total gas coverage constant at 60%.

Figure 4a displays our best fit model compared to the UVS-measured albedo. The best fit model included a thin ($N=4.0\times10^{17}$ cm^{-2}) SO_2 gas component overlying the SO_2 frost region, a thick ($N=1.0\times10^{19}$ cm^{-2}) SO_2 gas component overlying material of reflectance R_{other} = 0.032. The higher latitudes observed in the FOV were assumed to only contain the surface material of reflectance R_{other}, and no atmospheric component. In Figure 4b we show the three individual components of the model. The thick atmospheric component is important near 2350-2400 Å, where it adds a narrow local maximum to the model. As first pointed out by *Clarke et al.* [1994], the thick component is saturated out at most wavelengths in this range and provides only an emission feature near 2400 Å. Figure 4c displays the measured albedo and the model not including the thick gas component to demonstrate its effect near 2400 Å.

Uncertainties in the derived column densities were determined based on the goodness of fit of the model to the data. We found that the thick atmospheric component column density could vary by a factor of 2 before the quality of the fit was unsatisfactory; the range of best fit values is thus $N=5.0\times10^{18}$-$2.\times10^{19}$ cm^{-2}. For the thin component, satisfactory fits to the data were achieved for $N=3.\times10^{17}$-9.0×10^{17} cm^{-2}.

6. Discussion

Using Model 3, which incorporates a localized thick SO_2 atmosphere, SO_2 frost and an additional surface component with a flat reflectance, a good fit was obtained over the measured wavelength range (2100-3200 Å). In particular, the fit was improved in the 2250-2400 Å region, where thick SO_2 atmosphere accounts for an increase in the measured albedo.

6.1 Comparisons With Previous Results

The results presented here are consistent with those obtained by *Clarke et al.* [1994] using a HST GHRS spectrum in the same wavelength range; they found that a model including 10% coverage by $N=2\times10^{19}$ cm^{-2} and 90% coverage by $N=2\times10^{16}$ cm^{-2} was consistent with their data. Atmospheric thicknesses on the order of $N\sim1\times10^{18}$ cm^{-2} were obtained by *Sartoretti et al.* [1994, 1996] using HST FOC images also in

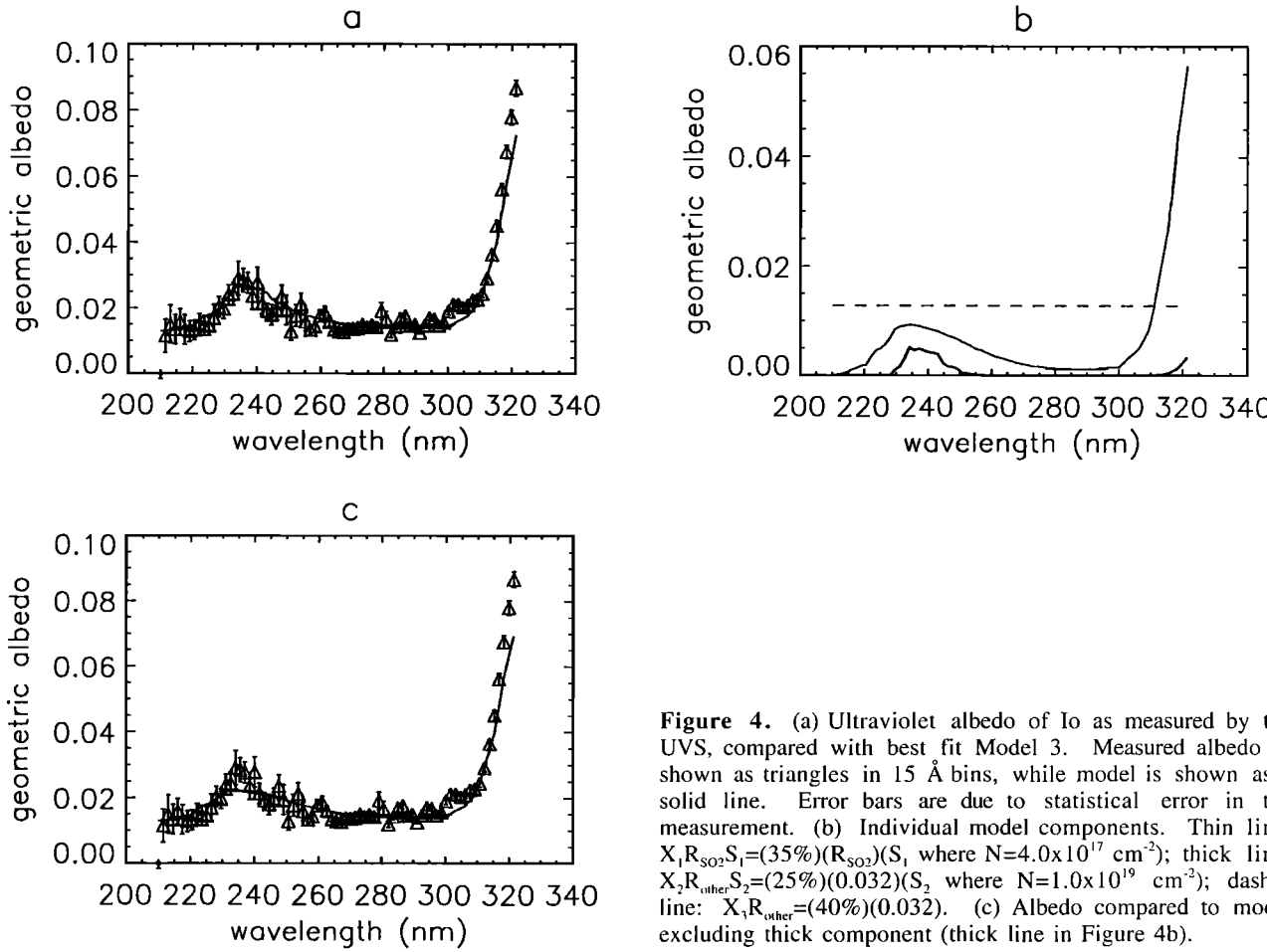

Figure 4. (a) Ultraviolet albedo of Io as measured by the UVS, compared with best fit Model 3. Measured albedo is shown as triangles in 15 Å bins, while model is shown as a solid line. Error bars are due to statistical error in the measurement. (b) Individual model components. Thin line: $X_1R_{SO2}S_1=(35\%)(R_{SO2})(S_1$ where $N=4.0x10^{17}$ cm^{-2}); thick line: $X_2R_{other}S_2=(25\%)(0.032)(S_2$ where $N=1.0x10^{19}$ cm^{-2}); dashed line: $X_3R_{other}=(40\%)(0.032)$. (c) Albedo compared to model excluding thick component (thick line in Figure 4b).

this wavelength range (2325 Å, 2600 Å, 2850 Å). The model presented here that is consistent with UVS data includes 35% coverage by an atmospheric component of $N=4.x10^{17}$ cm^{-2}. This "thin" component agrees with the column densities measured near 2100 Å in high-resolution HST specta by *Ballester et al.* [1994] and *Trafton et al.* [1996]. These comparisons indicate that the near-UV wavelengths (particularly near 2400 Å) are important in detecting column densities of $N\sim1x10^{18}$-$1x10^{19}$ cm^{-2}. Measurements near 2100 Å are vital in detecting column densities of $N\sim1x10^{16}$-$1x10^{17}$ cm^{-2}. These results are also consistent with the suggestion by *Lellouch* [1996] that different wavelength ranges detect SO_2 column densities of varying thicknesses. Near 2100 Å, a "thin" component is detectable, likely due to sublimation of surface frost. In millimeter wavelength observations, thicker gas components are detected, presumably due to volcanic plumes. We suggest that the near-UV wavelengths detect still a thicker SO_2 gas component, due to volcanic plumes and outgassing at hotspots (discussed below).

6.2 Implications

In our model we varied the thickness of coverage of the thick and thin atmospheric components. We tried letting the thick component cover the entire SO_2 frost region and having the thin component cover the other material. We tried letting the thick component cover part of the frost and the thin component cover the other part of the frost and part of the nonfrost region. We tried letting the thick component cover the nonfrost material and the thin component cover the frost.

We found that the best fit had the thicker gas component over the nonfrost material and the thinner gas component over the frost. This indicates that a thicker column density of SO_2 gas is associated with nonfrost regions. Several hot spots were included in the FOV in the nonfrost regions, and the Amirani plume was also included in the FOV. These results suggest that sublimation of surface frost produces a thin ($N\sim4x10^{17}$ cm^{-2}) atmospheric component, while outgassing from hot spots and volcanic plumes produces a thicker gas component ($N\sim1.0x10^{19}$ cm^{-2}). This may indicate that "stealth plumes" [*Johnson et al.*, 1995] are associated with these hot spots, contributing to the thick SO_2 gas component, where dust particulates are not included in the plumes, so they are undetectable at visible wavelengths.

7. Conclusions

The conclusions of this work may be summarized in the three following points.

1. Sulfur dioxide frost alone does not account for the shape of Io's albedo in the 2100-3200 Å wavelength range.

2. Sulfur dioxide gas must be included in the model of Io's near-ultraviolet albedo, and the gas must be in a thick localized region, not hemispherically homogeneous.

3. Our best fit model includes a thick atmospheric region covering 25% of the observed region with a column density $N \sim 1.0 \times 10^{19}$ cm^{-2}. Also important in fitting the near-UV data is a thinner atmospheric region of column density $N \sim 4.0 \times 10^{17}$ cm^{-2}. We find that the thinner SO_2 gas component is likely due to sublimation of SO_2 frost, while the thicker component is associated with volcanic plumes and outgassing at hotspots.

These results are consistent with previous high spectral resolution observations near 2100 Å which indicated column densities of $N \sim 3 \times 10^{17}$ cm^{-2} [*Ballester et al.*, 1994; *Trafton et al.*, 1996]; they are also consistent with earlier near-UV observations which indicated column densities of $N \sim 1.5 \times 10^{19}$ cm^{-2} in localized regions [*Clarke et al.*, 1994]. Put together, these observations all indicate that different regions of the ultraviolet detect different SO_2 gas thicknesses due to the strong variation in wavelength that the SO_2 cross section exhibits for different column densities. This is in agreement with the suggestion by *Lellouch* [1996] that observations performed in varying wavelength ranges detect different parts of Io's atmosphere.

Acknowledgments. M. Belton and an anonymous reviewer provided constructive comments. Many thanks to W. K. Tobiska, K E. Simmons, W. Sweet, and J. Gebben for assistance with observations and data; A. McEwen for information on SSI results, B. Knapp for the SOLSTICE solar spectrum. A.R.H. is grateful for helpful discussions with M McGrath and G. Ballester.

References

Ballester, G. E., D. F Strobel, H. W. Moos, and P. D. Feldman, The atmospheric abundance of SO_2 on Io, *Icarus, 88*, 1-23, 1990.

Ballester, G. E., M A. McGrath, D. F. Strobel, X. Zhu, P D. Feldman, and H. W. Moos, Detection of the SO_2 atmosphere on Io with the Hubble Space Telescope, *Icarus, 111*, 2-17, 1994.

Belton, M. J. S., An interpretation of the near-ultraviolet absorption spectrum of SO_2: Implications for Venus, Io, and laboratory measurements, *Icarus, 52*, 149-165, 1982.

Bertaux, J. L., and M J. S. Belton, Evidence of SO_2 on Io from UV observations, *Nature, 282*, 813-815, 1979.

Butterworth, P S., J. Caldwell, V. Moore, T. Owen, A R Rivolo, and A. L. Lane, An upper limit to the global SO_2 abundance on Io, *Nature, 285*, 308-309, 1980.

Carlson, R. W., et al., The distribution of sulfur dioxide and other infrared absorbers on the surface of Io, *Geophys. Res. Lett*, *24*, 2479-2482, 1997.

Clarke, J. T., J. Ajello, J. Luhmann, N. Schneider, and I. Kanik, Hubble Space Telescope UV spectral observations of Io passing into eclipse, *J. Geophys. Res*, *99*, 8387-8402, 1994.

Cruikshank, D P., T. J. Jones, and C. B. Pilcher, Absorption bands in the spectrum of Io, *Astrophys. J., 225*, L89-L92, 1978.

Fanale, F. P, R. H. Brown, D. P. Cruikshank, and R. N. Clark, Significance of absorption features in Io's IR reflectance spectrum, *Nature, 280*, 761-763, 1979.

Hapke, B, *Theory of Reflectance and Emittance Spectroscopy*, Cambridge Univ. Press, New York, 1993.

Hendrix, A. R., The Galileo ultraviolet spectrometer: In-flight calibration and ultraviolet albedos of the Moon, Gaspra, Ida and Europa. Ph.D. thesis, Univ. of Colo., Boulder, 1996.

Hendrix, A. R., et al., Galileo ultraviolet spectrometer observations of Io (abstract), *Eos Trans. AGU, 77*, Fall. Meet. Suppl., F437, 1996.

Hendrix, A. R., C. A. Barth, C. W. Hord, A. I. F. Stewart, K. E. Simmons, W. E McClintock, J. M. Ajello, and A. L. Lane, Io: Surface and atmosphere observations by the Galileo ultraviolet spectrometer (abstract), *Eos Trans. AGU, 78* (46), Fall Meet. Suppl., F418, 1997.

Hord, C. W., et al., Galileo ultraviolet spectrometer experiment, *Space Sci. Rev., 60*, 503-530, 1992.

Howell, R. R., D. B. Nash, T. R. Geballe, and D. P. Cruikshank, High-resolution infrared spectroscopy of Io and possible surface materials, *Icarus, 78*, 27-37, 1989.

Johnson, T. V , D. L. Matson, D L. Blaney, and G. J. Veeder, Stealth plumes on Io, *Geophys. Res. Lett., 22*, 3293-3296, 1995.

Lellouch, E., Io's atmosphere: Not yet understood, *Icarus, 124*, 1-21, 1996.

Lellouch, E., M. Belton, I. DePater, G. Paubert, S. Gulkis, and T. Encrenaz, The structure, stability, and global distribution of Io's atmosphere, *Icarus, 98*, 271-295, 1992.

Lopes-Gautier, R., A. G. Davies, R. Carlson, W. Smythe, L. Kamp, L. Soderblom, F. E. Leader, R. Mehlman, and Galileo NIMS team. Hot spots on Io: Initial results from Galileo's near infrared mapping spectrometer, *Geophys. Res. Lett.. 24*, 2439-2442, 1997.

Manatt, S. L., and A. L. Lane, A compilation of SO_2 absorption cross sections from 106-403 nm, *J. Quant. Spectrosc. Radiat. Transfer, 50*, 267-276, 1993.

McEwen, A. S., T. V. Johnson, D. L. Matson, and L A. Soderblom, The global distribution, abundance, and stability of SO_2 on Io, *Icarus, 75*, 450-478, 1988.

Nash, D. B , F. P. Fanale, and R. M. Nelson, SO_2 frost: UV-visible reflectivity and Io surface coverage, *Geophys. Res. Lett., 7*, 665-668, 1980.

Pearl, J. C., R. Hanel, V. Kunde, W. Maguire, D. Fox, S. Gupta, C. Ponnamperuma, and F. Raulin, Identification of gaseous SO_2 and new upper limits for other gases on Io, *Nature, 280*, 755-758, 1979.

Pollack, J. B., F. C. Witteborn, E. F. Erickson, D. W. Strecker, B. J. Baldwin, and T E. Bunch, Near-infrared spectra of the Galilean satellites: Observations and compositional implications, *Icarus, 36*, 271-303, 1978.

Rottman, G. J., T. N. Woods, and T. P. Sparn, Solar-Stellar Irradiance Comparison Experiment, 1, Instrument design and operation, *J. Geophys. Res., 98*, 10667-10677, 1993.

Sartoretti, P., M. A. McGrath, and F. Paresce, Disk-resolved imaging of Io with the Hubble Space Telescope, *Icarus, 108*, 272-284, 1994.

Sartoretti, P., M. J. S. Belton, and M. A. McGrath, SO_2 distributions on Io, *Icarus, 122*, 273-287, 1996.

Simonelli, D. P., and J. Veverka, Voyager disk-integrated photometry of Io, *Icarus, 59*, 406-425, 1984.

Simonelli, D. P , and J. Veverka, Phase curves of materials on Io: Interpretation in terms of Hapke's function, *Icarus, 68*, 503-521, 1986.

Smythe, W. D., R. M. Nelson, and D. B. Nash, Spectral evidence for SO_2 frost or adsorbate on Io's surface, *Nature, 280*, 766, 1979.

Trafton, L. M., J. J. Caldwell, C. Barnet, and C. C. Cunningham, The gaseous sulfur dioxide abundance over Io's leading and trailing hemispheres: HST spectra of Io's C^1B_2-X^1A_1 band of SO_2 near 2100 Å, *Astrophys. J., 456*, 384-392, 1996.

Wagner, J K., B. W. Hapke, and E. N. Wells, Atlas of reflectance spectra of terrestrial, lunar and meteoritic powders and frosts from 92 to 1800 nm, *Icarus, 69*, 14-28, 1987.

A. R. Hendrix, C. A. Barth, and C. W. Hord, Laboratory for Atmospheric and Space Physics, University of Colorado, Campus Box 590, Boulder, CO 80309-0590. (hendrix@lasp.colorado.edu)

(Received July 15, 1998, revised January 29, 1999;
accepted February 10, 1999.)